Supplementary information

Ion sieving membrane for direct seawater anti-precipitation hydrogen evolution reaction electrode

Qianfeng Liu, Zhao Yan, Jianxin Gao, Hefei Fan, Min Li and Erdong Wang*

Dalian National Laboratory for Clean Energy, Dalian Institute of Chemical Physics, Chinese Academy of Sciences, Dalian 116023, China
* Corresponding author.

E-mail: edwang@dicp.ac.cn

Experimental

Materials

Nickel chloride ($NiCl_2·6H_2O$, ≥98.0%), cobalt chloride ($CoCl_2·6H_2O$, ≥99.0%), ferrous chloride ($FeCl_2·4H_2O$, ≥98.0%), magnesium chloride ($MgCl_2·6H_2O$, ≥98.0%), calcium chloride ($CaCl_2$, ≥96.0%), aluminium chloride ($AlCl_3·6H_2O$, ≥97.0%), potassium chloride (KCl, ≥99.5%), sodium chloride (NaCl, ≥99.5%), sodium hydroxide (NaOH, ≥96.0%), magnesium hydroxide ($Mg(OH)_2$, 98%-102%), sodium sulphate (Na_2SO_4, ≥99.0%), sodium carbonate (Na_2CO_3, ≥99.8%), sodium nitrate ($NaNO_3$, ≥99.0%), hydrochloric acid (HCl, 37%), acetone (CH_3COCH_3, ≥99%) and chloroplatinic acid ($H_4PtCl_6·6H_2O$, Pt = 37%) were obtained from Sinopharm Chemical, Tianjing or Nanjing Reagent. All the chemicals were used as received without purification. Nickel foam (thicknesses: 1.7 mm, density: 320 g cm^{-2}, pore size: 110 PPI) was obtained from Heze Tianyu Technology Development Co., Ltd. Nylon filter membrane (pore size of 0.45 μm, membrane diameter of Φ50 mm) was purchased from Green Mall. Iridium and ruthenium oxide covered titanium felt ($IrRuO_2$-Ti, Ir:Ru=1:2, with total mass of 12 g/m^2) was obtained from Kunshan. Seawater was obtained from Dalian, Liaoning province.

Samples preparation

In a typical synthesis for $Ni(OH)_2$-NF electrodes, NFs (1 cm × 2 cm) were pre-treated with acetone via ultrasonic cleaning for 15 min and dried at 40°C for 1 hour, followed by ultrasonic cleaning with 3 M HCl for 10 min, and washing with RO water for several times. The wet NFs were immersed in 0.1 M $NiCl_2$ solution and kept at 25°C for 1 d to 5 d, marked as $Ni(OH)_2$-NF-1d to $Ni(OH)_2$-NF-5d. The obtained $Ni(OH)_2$-NF electrodes were washed with RO water for several times and stored in RO water before use. The FeOOH/NF, $Co(OH)_2$/NF, Ni_2Fe_1 LDH/NF, Ni_2Co_1 LDH/NF, Mg_2Al_1 LDH/NF electrodes were fabricated via the similar condition to $Ni(OH)_2$-NF-3d, the difference was the $NiCl_2$ solution was replaced by $FeCl_2$, $CoCl_2$, $MgCl_2$, or $AlCl_3$ with total concentration of 0.1 M. The prepared method of $Ni(OH)_2$-NS-NF electrode and Pt-NF electrode was obtained from our previous work.[1] The $Ni(OH)_2$-Pt-NF electrode was fabricated from Pt-NF electrode with the same condition to $Ni(OH)_2$-NF electrode.

$Ni(OH)_2$ membrane preparation

The $Ni(OH)_2$ membrane was peeled off from abundant $Ni(OH)_2$-NF electrodes via ultrasound over 24 h, then centrifuged and washed with ultra-pure water for several times. The obtained $Ni(OH)_2$ was dispersed in water with concentration about 1wt.%. 5 mL of $Ni(OH)_2$ stirring

turbid liquid was diluted into 80 mL and vacuum filtrated on nylon filter membrane to fabricate the $Ni(OH)_2$ membrane with working size of Φ40 cm. Before permeability test, the $Ni(OH)_2$ membrane was sealed with a 2 cm^2 opening in copper tape to control the ions transfer area.

Characterization

The crystal structures were characterized by X-ray diffraction (XRD, Rigaku MiniFlex 600, 40 kV, 15 mA) using Cu Kα1 radiation at a scanning rate of 5° min^{-1}. The microscopic features of the samples were characterized by scanning electron microscopy (SEM, JEOL JSM-7800F and Hitachi S-5500) coupled with energy-dispersive X-ray spectroscopy (EDS, Oxford X-Max) and high-resolution transmission electron microscopy (HRTEM, JEOL JEM-2100, 200 kV). X-ray photoelectron spectroscopy (XPS) analysis was conducted on an Thermo Scientific K-Alpha X-ray photoelectron spectrometer (Thermo Fisher Scientific Inc.) with Al Kα radiation in an ultrahigh vacuum. Zeta potential of the sample was measured by the nano laser particle size analyser (Zetasizer Nano, Malvern Panalytical) in 3.5% NaCl solution at pH of 10, which was adjusted by 1 M NaOH solution.

Permeability of Ions

The permeability of the ions was tested by a diffusion cell. The feed solution: 1 mol L^{-1} aqueous solution with ultra-pure water, including KCl, NaCl, $CaCl_2$, $MgCl_2$, NaOH, $NaNO_3$, Na_2CO_3 and Na_2SO_4 with a varied hydrated diameter of cations or anions, respectively. The concentration of $MgCl_2$ and NaOH solution also included 0.1, 0.3, 0.5 and 0.75 M. The permeate side: ultra-pure water. The ion concentration of the diffusion side was then calculated by following equation (Fig. S20).

$$\lg(\sigma) = a + \lg(c) \qquad (1)$$

σ is the conductivity of the solution, c is the concentration of the solution.

Electrochemical measurements

Electrochemical measurements were carried out on CHI 760D electrochemical workstation in a traditional three-electrode cell at 25 ±1°C. The NF, $Ni(OH)_2$-NF, Pt-NF or $Ni(OH)_2$-Pt-NF as the working electrode (WE) with an effective projected area of 0.5 cm^2, pure Mg rod as the counter electrode (CE) and a double-salt-bridge saturated calomel electrode (SCE) as the reference electrode was measured in seawater or seawater with saturated $Mg(OH)_2$. The saturated $Mg(OH)_2$ seawater was obtained by adding of ~0.2 g $Mg(OH)_2$ powder into 1 L seawater and kept stirring for one night. The volume of the electrolyte was 40 mL for each

chamber when the WE and CE was separated with AEM. All polarization curves were recorded at a scanning rate of 5 mV s^{-1} with iR-compensation unless otherwise noted.

Directly seawater electrolyser measurements

The directly seawater electrolyser was assembled by prepared $Ni(OH)_2$-Pt-NF or Pt-NF HER electrode and Cr_2O_3-$IrRuO_2$-Ti OER electrode with working area of 10 cm^2. The Cr_2O_3 layer on the $IrRuO_2$-Ti (Cr_2O_3-$IrRuO_2$-Ti) was fabricated with the same condition to the reference.[24] The diaphragm was the commercial PP/PE membrane with thickness of 210 μm. The seawater electrolyser under 40°C was flowed by seawater with saturated $Mg(OH)_2$ at a rate of 12 mL min^{-1} under control of a peristaltic pump.

Magnesium seawater battery measurements

The MSWB was assembled by $Ni(OH)_2$-Pt-NF, Pt-NF or NF cathode and Mg alloy (AZ31) anode with working size of 2 × 2 cm^2. The distance between cathode and anode was 0.5 mm, and there was no diaphragm between the electrodes. All the MSWBs were tested in seawater with saturated $Mg(OH)_2$. Before the polarization test, the MSWBs were tested at current density of 5 mA cm^{-2} for 5 min to reach a stable potential, and the test time for each current density point in i-V curves was 2 min. The precipitation mass on the electrodes were calculated by the mass difference of electrodes before and after discharge measurement.

Simulations

A monolayer $Ni(OH)_2$ nanosheet with 0 charge or +10 electronic charge was built by 13 × 11 Ni atoms as framework, which contained a 5 × 3 Ni atoms (1.1 × 1.4 nm^2) opening in the centre of the nanosheet. To simulate the transfer rate of Mg^{2+}, Na^+, Cl^-, OH^- and H_2O, and avoid the deposition influence between Mg^{2+} and OH^-, the simulation was divided into $MgCl_2$ and NaOH solution system. The $MgCl_2$ and NaOH solution was up to the $Ni(OH)_2$ sheet at 300 K and 1 atm in a box with size of 3.0×4.0×12.0 nm^3. The $MgCl_2$ solution contained 3000 H_2O, 40 Mg^{2+} and 80 Cl^-, while NaOH solution contained 3000 H_2O, 40 Na^+ and 40 OH^-. The $Ni(OH)_2$ sheets were set as rigid to ensure that the atoms of the substrates were fixed during the simulation. The temperature of each confined solution was maintained at 300 K by using a Nosé–Hoover thermostat with a damping factor of 100 fs. The solutions were allowed to equilibrate for 10 ns with a time step of 1 fs by using NVT simulations. Then, another 7 ns of simulation was performed for further analysis, and let particles and ions across through the opening on $Ni(OH)_2$ sheet driven by a transparent wall with 1 atm pressure on the top of the system. In also cases, the water transfer was referred to the tip3p model, the ions transfer and $Ni(OH)_2$ potential parameters were from the reports.[2-4] The Lorentz–Berthelot mixing rule was

adopted for the van der Waals interactions of different kinds of atoms. And all the passed ion and water numbers was counted by the LAMMPS software package.[55]

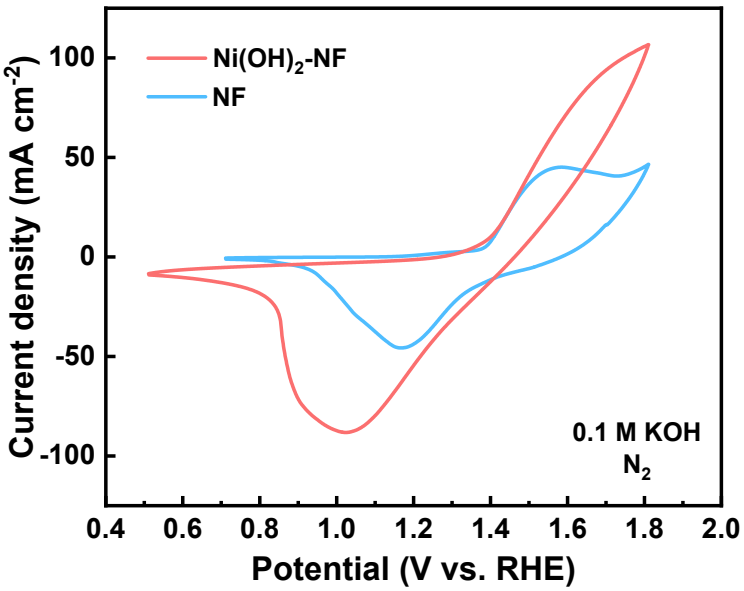

Fig. S1 CV curves of NF and $Ni(OH)_2$-NF electrode tested in N_2 saturated 0.1 M KOH at scan rate of 50 mV s^{-1}.

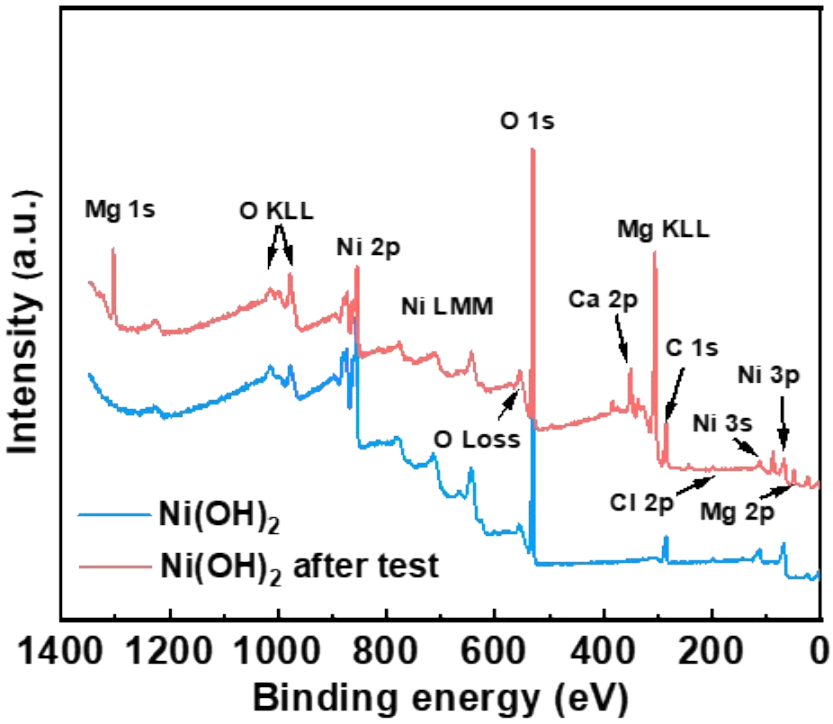

Fig. S2 XPS survey spectra of $Ni(OH)_2$ membrane before and after test in seawater.

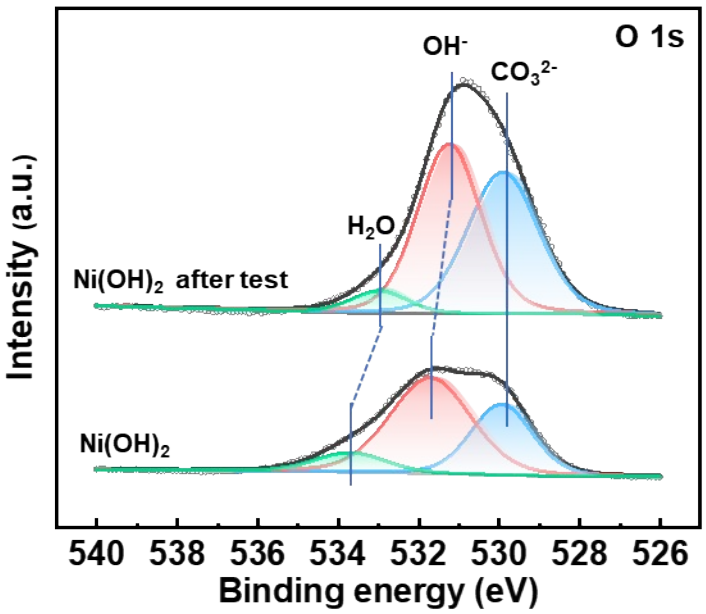

Fig. S3 High-resolution XPS spectra for O 1s of $Ni(OH)_2$ membrane before and after test in seawater.

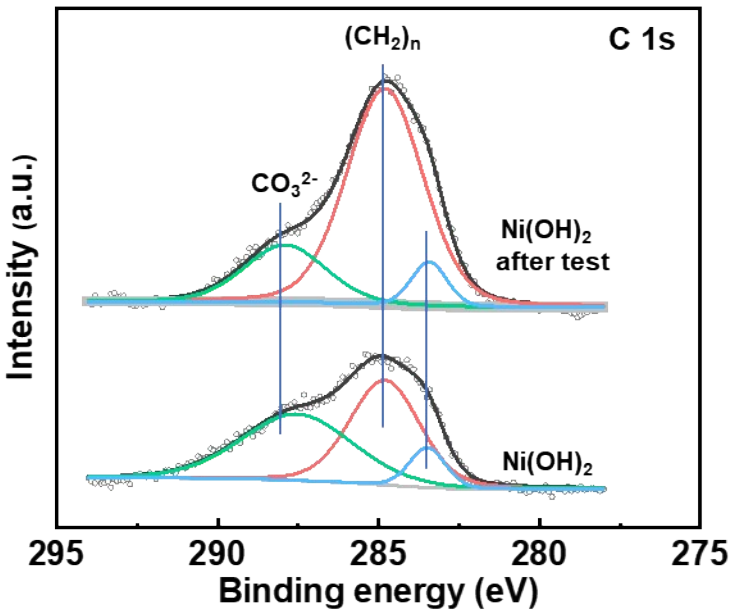

Fig. S4 The high-resolution XPS spectra of C 1s for $Ni(OH)_2$ membrane on $Ni(OH)_2$-NF electrode before and after test in seawater. The binding energy at 284.8 eV was chosen as the correction value.

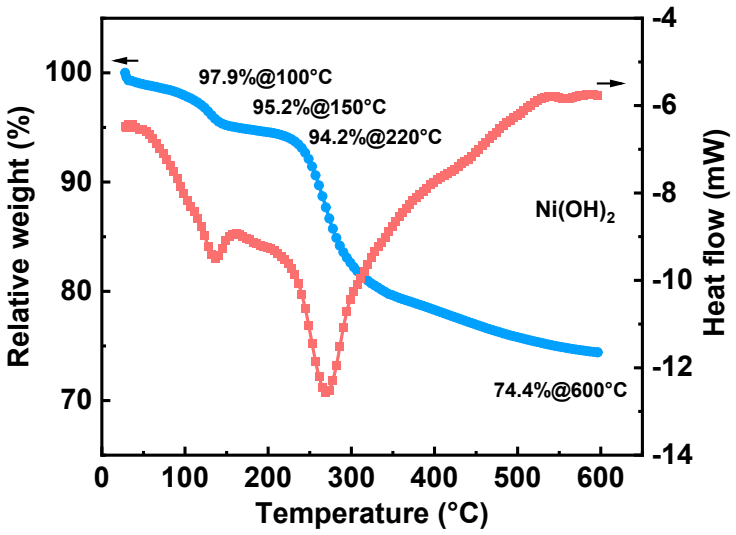

Fig. S5 Thermal gravimetric analysis of the $Ni(OH)_2$ membrane.

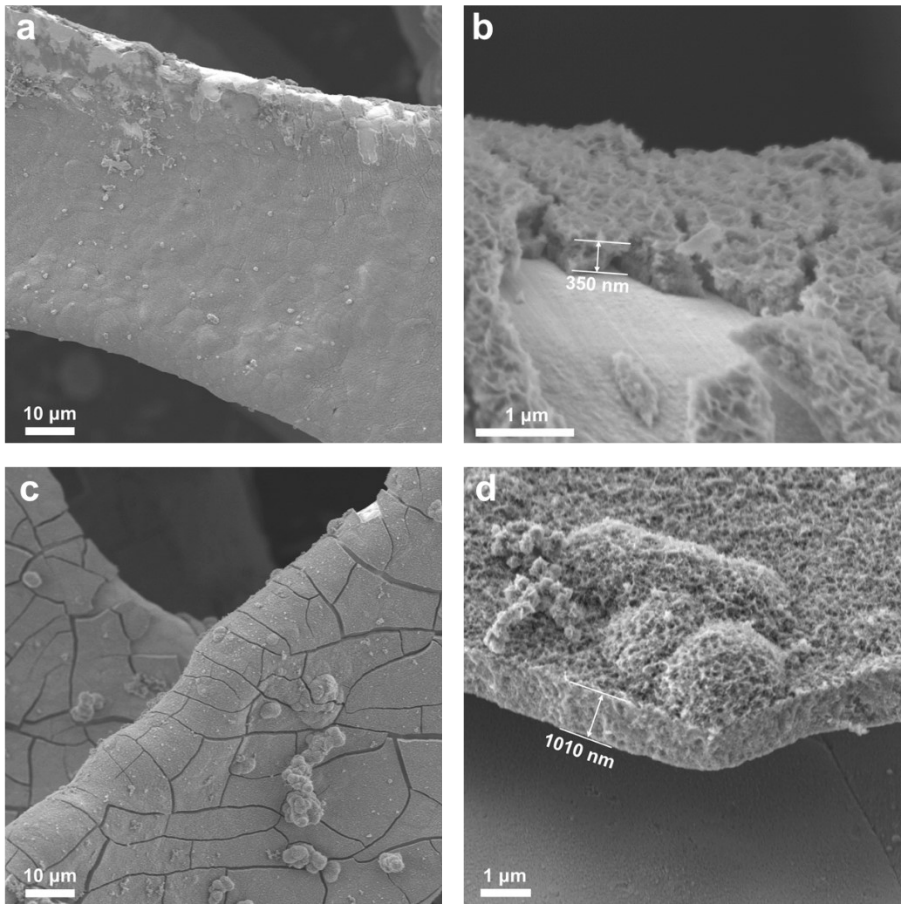

Fig. S6 SEM images of (a, b) $Ni(OH)_2$-NF-1d, and (c, d) $Ni(OH)_2$-NF-5d electrodes.

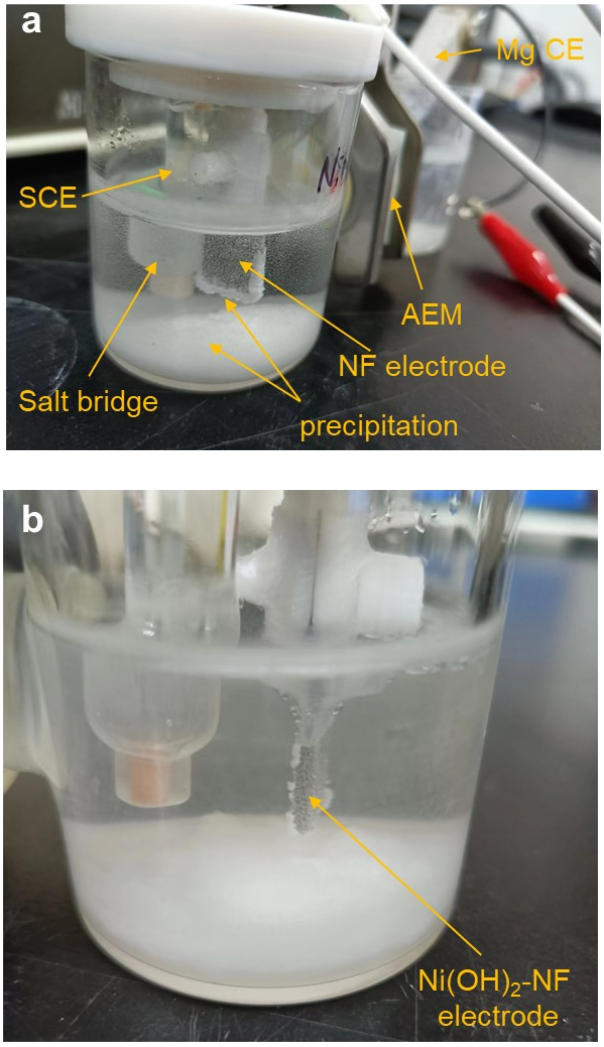

Fig. S7 Photograph of (a) NF and (b) $Ni(OH)_2$-NF electrode during test.

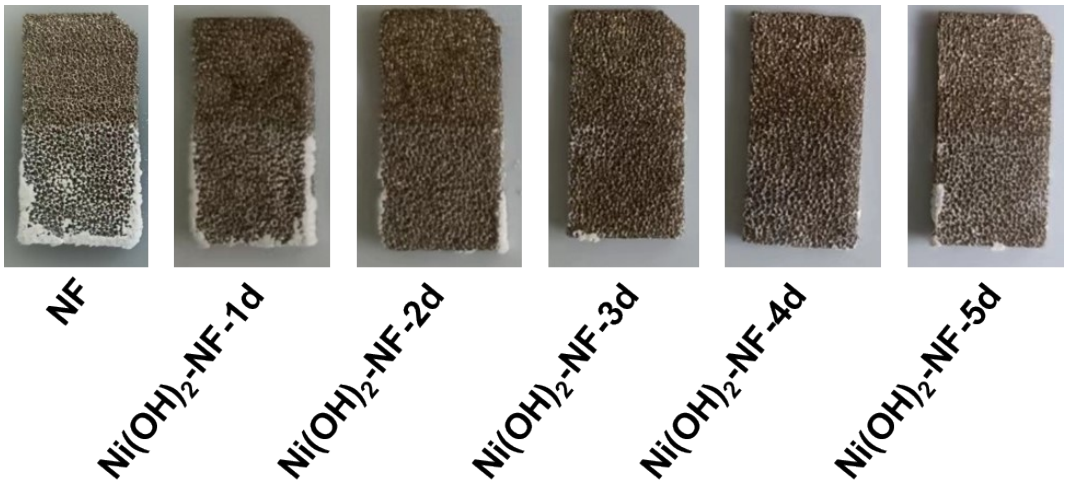

Fig. S8 Photograph of NF and $Ni(OH)_2$-NF electrodes after being tested in SW+AEM at current density of 10 mA cm^{-2} for 12 h.

The upper of the electrodes were protected by the PTFE film to prevent the contact between the electrodes with electrolyte, so the upper of the electrodes were not the reaction area for the electrodes.

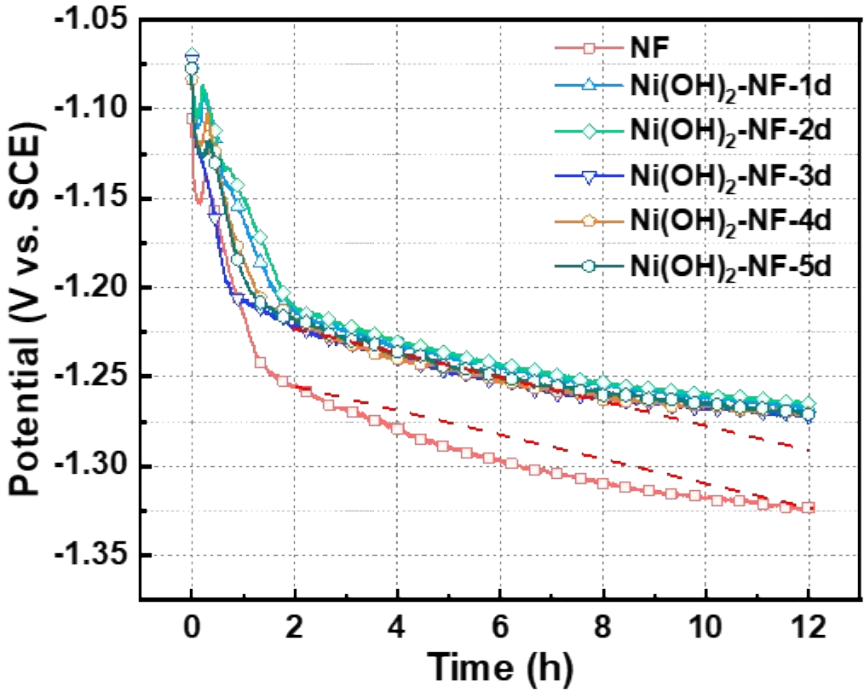

Fig. S9 Chronopotentiometry curves of NF and $Ni(OH)_2$-NF electrodes in SW+AEM at current density of 10 mA cm^{-2} for 12 h.

The rapid dropped potential for all electrodes was mainly caused by the zooming pH during the initial ~2 h measure. According to the parallel red dashed line from 2 to 12 h, the increased overpotential of $Ni(OH)_2$-NF electrodes was less than that of NF electrode with the same condition, indicating that the electrode surface $Ni(OH)_2$ membrane can promote its stability.

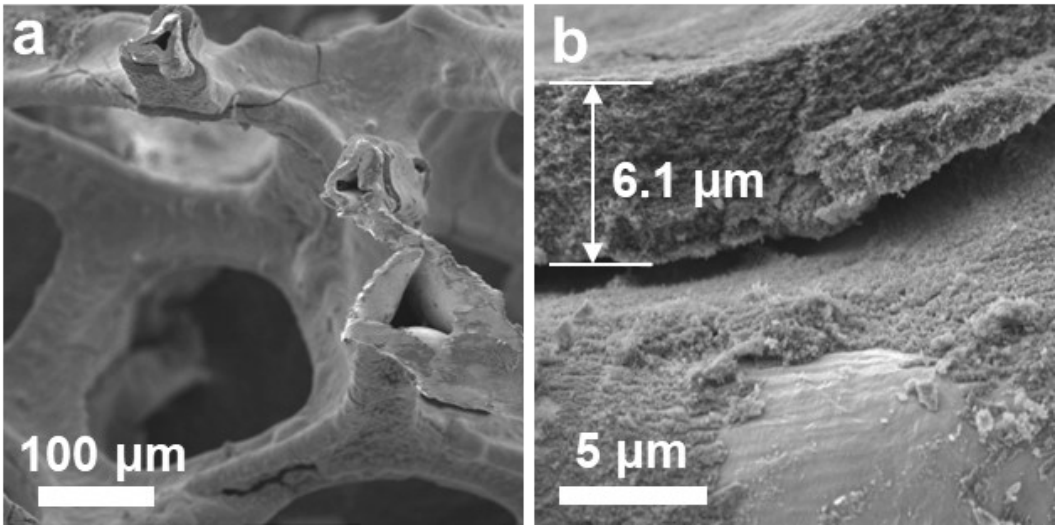

Fig. S10 SEM images of $Ni(OH)_2$-NF-3d electrode after tested in seawater at current density of 10 mA cm^{-2} for 12 h, the working electrode and counter electrode was separated with AEM.

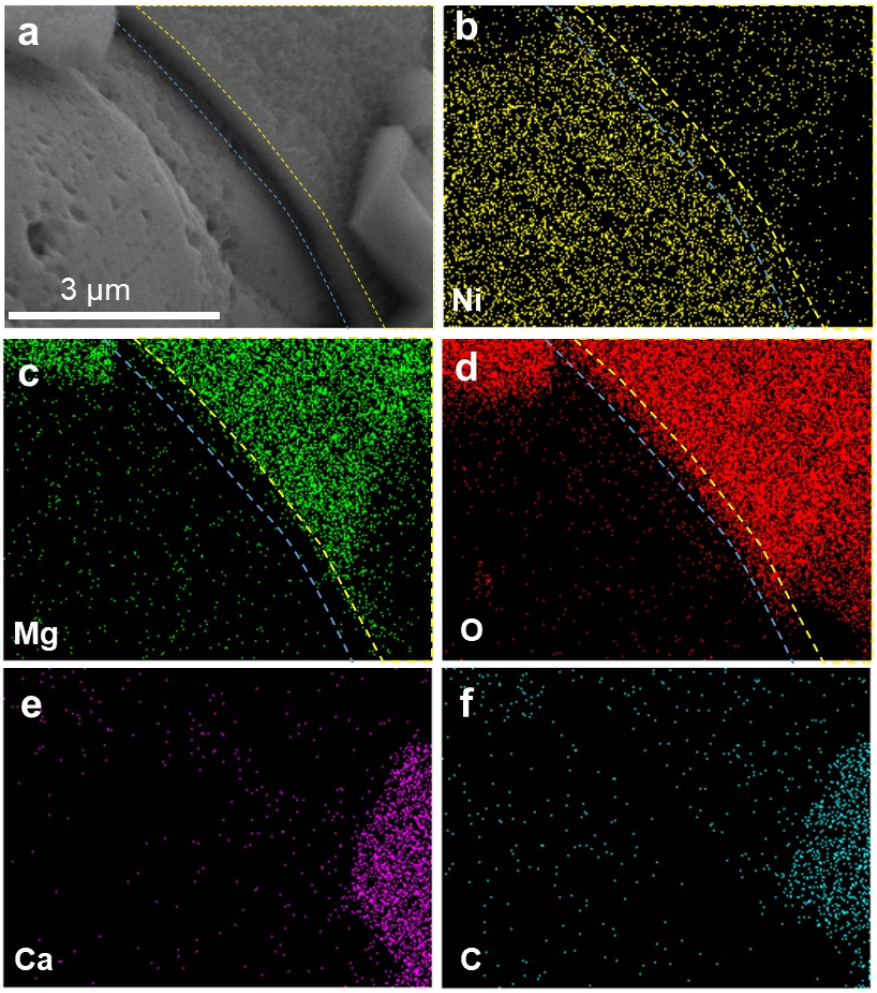

Fig. S11 a) SEM image and the corresponding energy-dispersive X-ray spectroscopy (EDS) elemental mapping of b) Ni, c) Mg, d) O, e) Ca and f) C for $Ni(OH)_2$-NF-3d electrode after tested in seawater at current density of 10 mA cm^{-2} for 12 h, the working electrode and counter electrode was separated with AEM.

The yellow and blue dashed lines were located at the same position at each image. It is the NF substrate below the blue line, it is the $Ni(OH)_2$ membrane between the two lines, and it is the Mg-based compound up the yellow line. According to the EDS elemental mapping, the Mg-based compound was mainly precipitated upon the $Ni(OH)_2$ membrane, suggesting the outstanding inhibition effect of Mg^{2+} transfer in $Ni(OH)_2$ membrane.

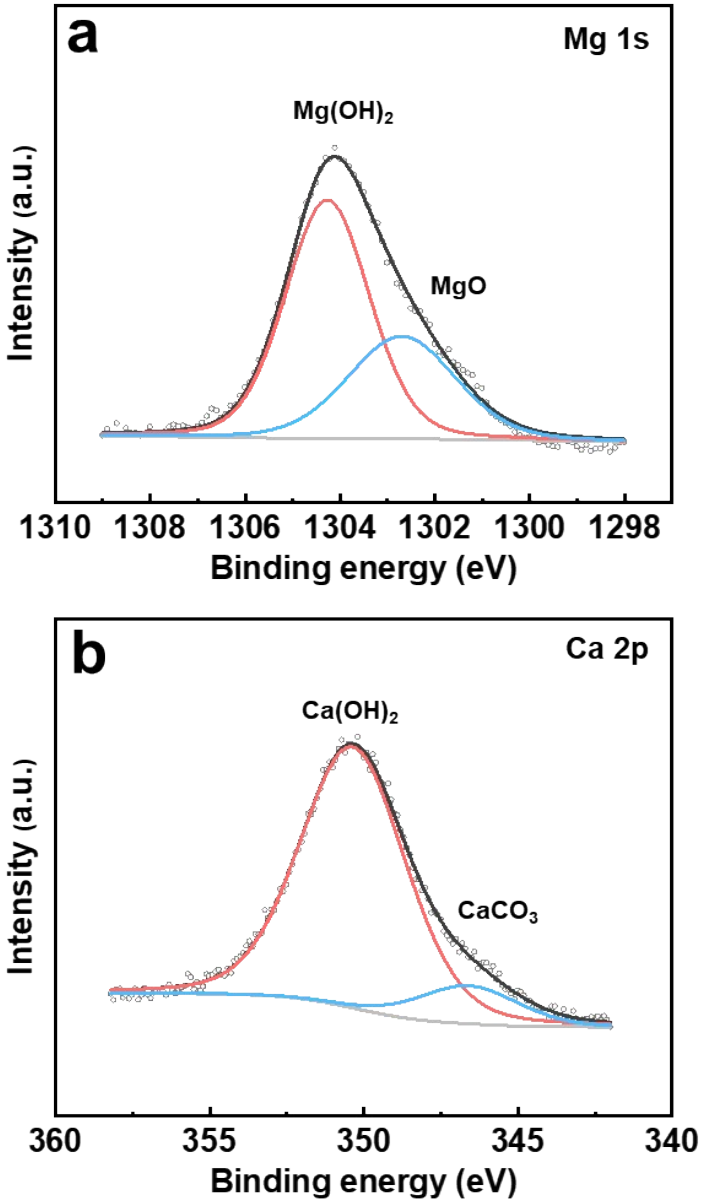

Fig. S12 High-resolution XPS spectra for (a) Mg 1s and (b) Ca 2p.

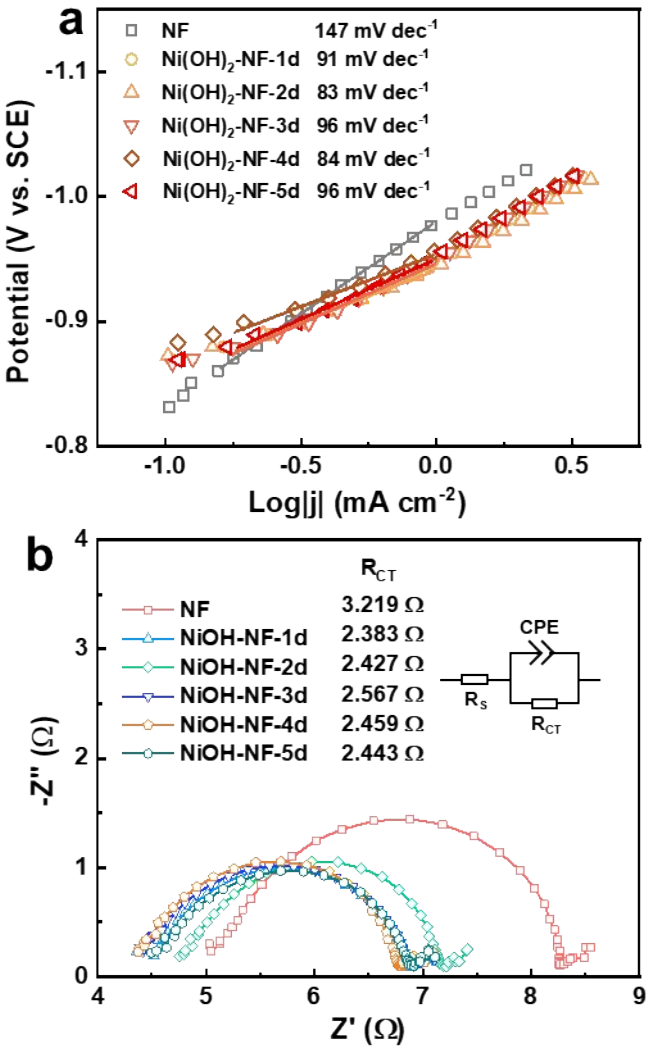

Fig. S13 (a) Tafel slopes and (b) electrochemical impedance spectroscopy (EIS) of NF and $Ni(OH)_2$-NF electrodes in SW+AEM.

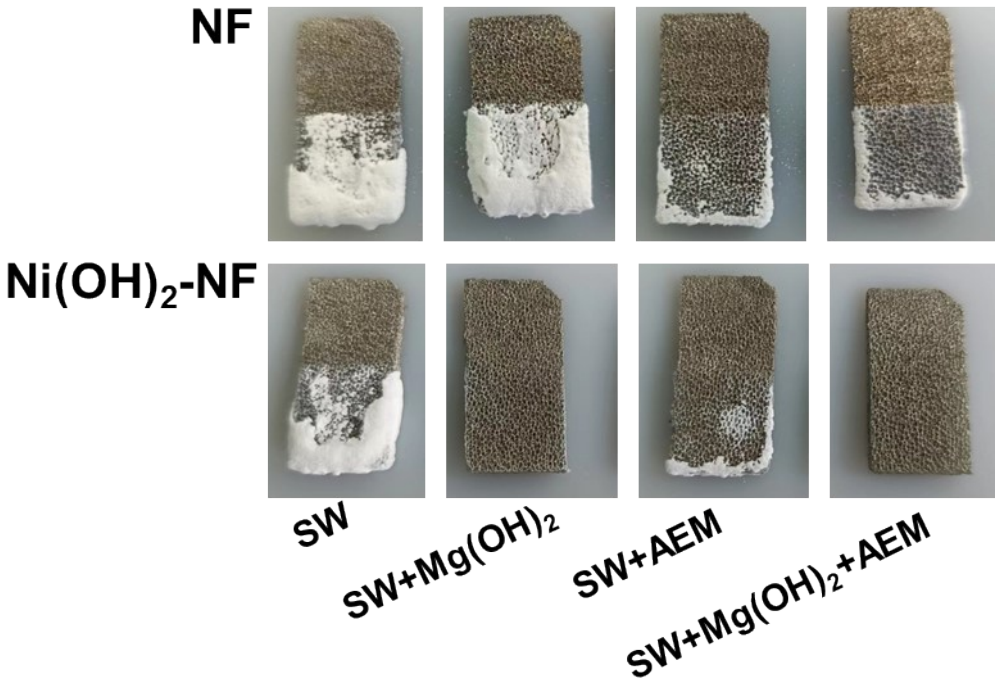

Fig. S14 Photographs of NF and $Ni(OH)_2$-NF electrodes after measurement under different conditions at 10 mA cm^{-2} for 12 h.

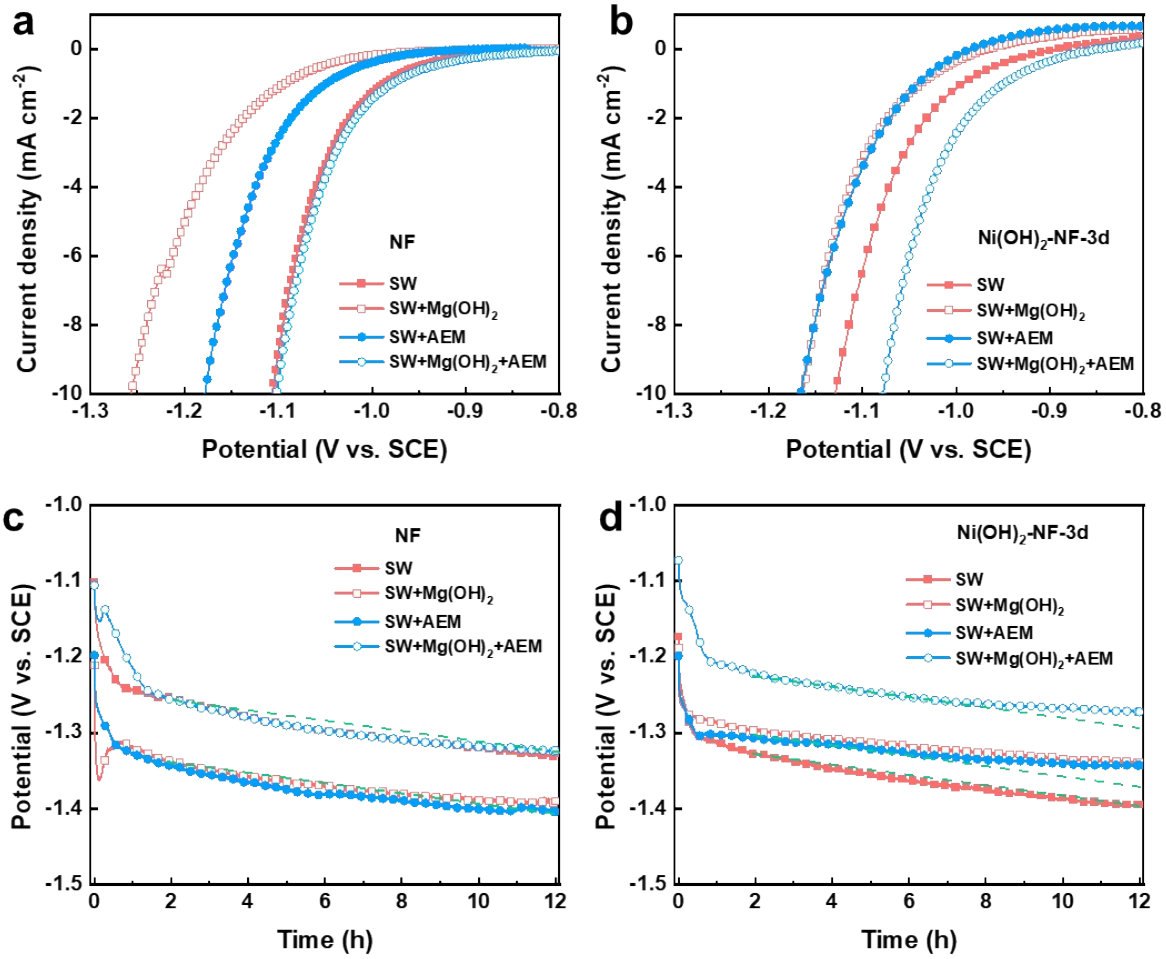

Fig. S15 LSV curves of (a) NF and (b) $Ni(OH)_2$-NF-3d electrode, and chronopotentiometry curves at 10 mA cm^{-2} of (c) NF and (d) $Ni(OH)_2$-NF-3d electrode measurement under different conditions.

According to the parallel dashed line from 2 to 12 h, the increased overpotential of $Ni(OH)_2$-NF electrode was less than that of NF electrode under different conditions, except for in SW, which was in accord with the precipitation mass on the electrode surface.

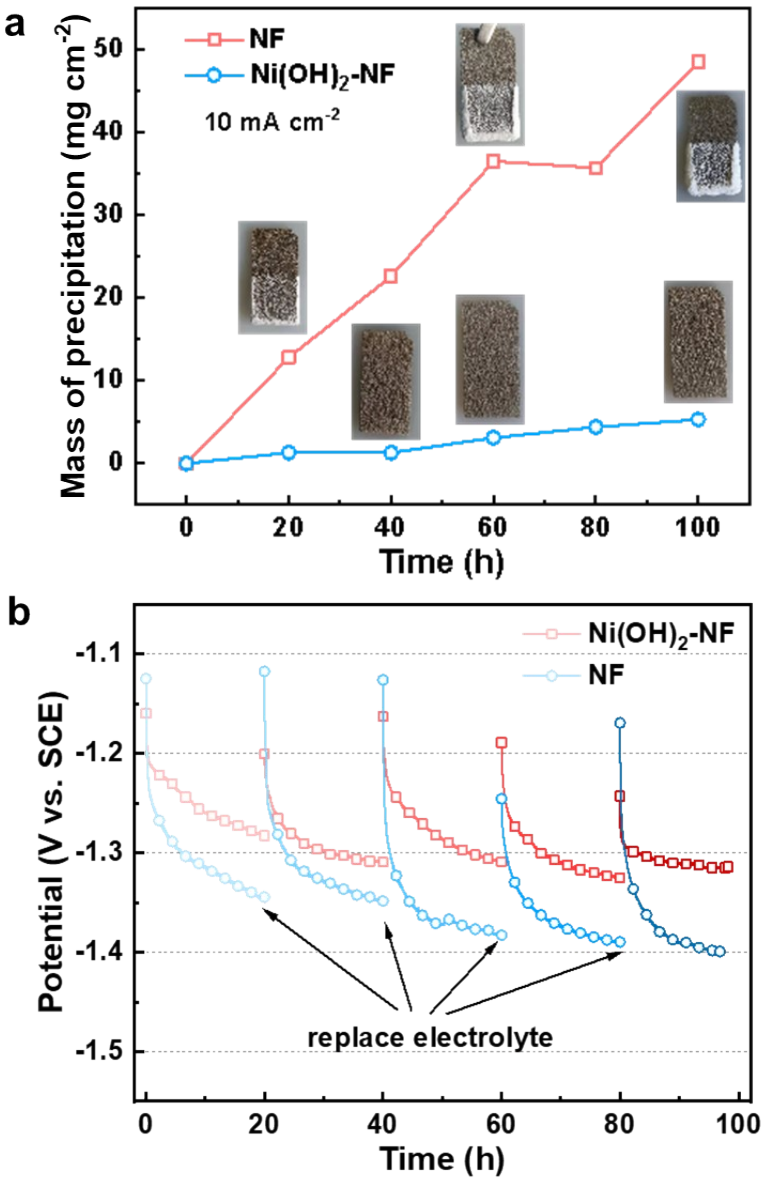

Fig. S16 (a) Mass of precipitation and (b) chronopotentiometry curves on the NF and $Ni(OH)_2$-NF electrodes under different measure time at current density of 10 mA cm^{-2}, the working electrode and counter electrode was separated with AEM, insets were the corresponding photographs.

The reduced precipitation mass for NF electrode at 80 h was mainly caused by the fall off during wash and dry.

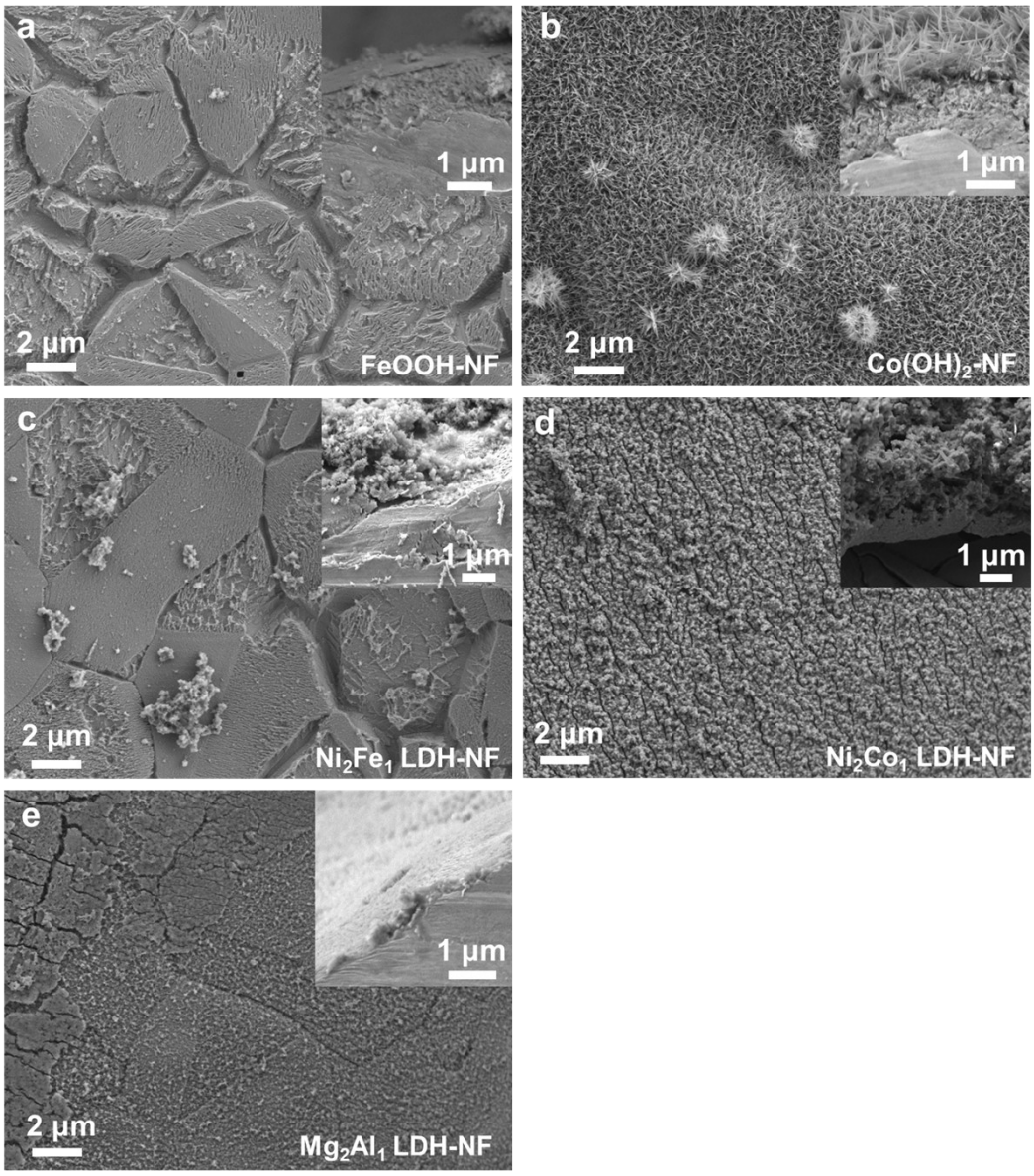

Fig. S17 SEM images of (a) FeOOH-NF, (b) $Co(OH)_2$-NF, (c) Ni_2Fe_1 LDH-NF, (d) Ni_2Co_1 LDH-NF, and (e) Mg_2Al_1 LDH-NF electrodes.

The membranes on FeOOH-NF, Ni_2Fe_1 LDH-NF and Mg_2Al_1 LDH-NF electrode were uneven, which led to much of exposed NF substrate. The membrane on $Co(OH)_2$-NF electrode was uniform but needlelike, which might supply much nucleating sites for $Mg(OH)_2$. The Ni_2Co_1 LDH-NF electrode generated the uniform membrane like $Ni(OH)_2$ membrane with thickness of 3.3 μm.

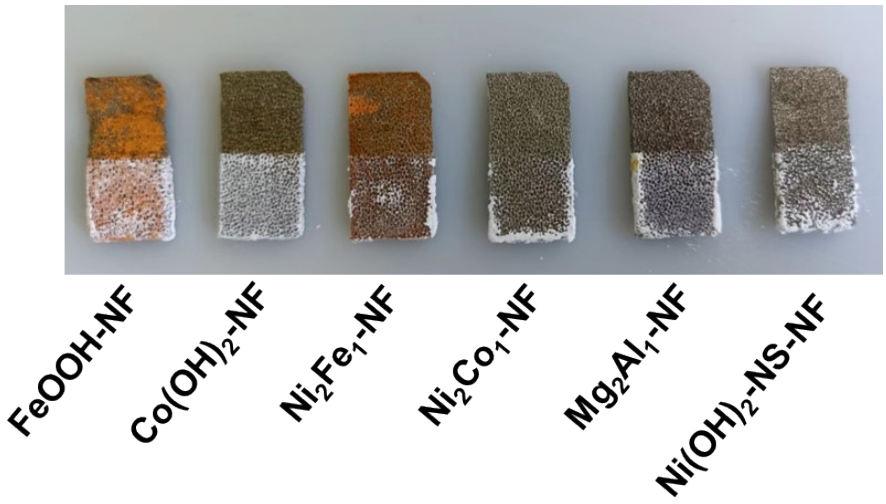

Fig. S18 Photogragh of FeOOH/NF, Co(OH)2/NF, Ni_2Fe_1 LDH/NF, Ni_2Co_1 LDH/NF, Mg_2Al_1 LDH/NF, and $Ni(OH)_2$-NS-NF electrodes after measurement at current density of 10 mA cm^{-2} for 12 h, the working electrode and counter electrode was separated with AEM.

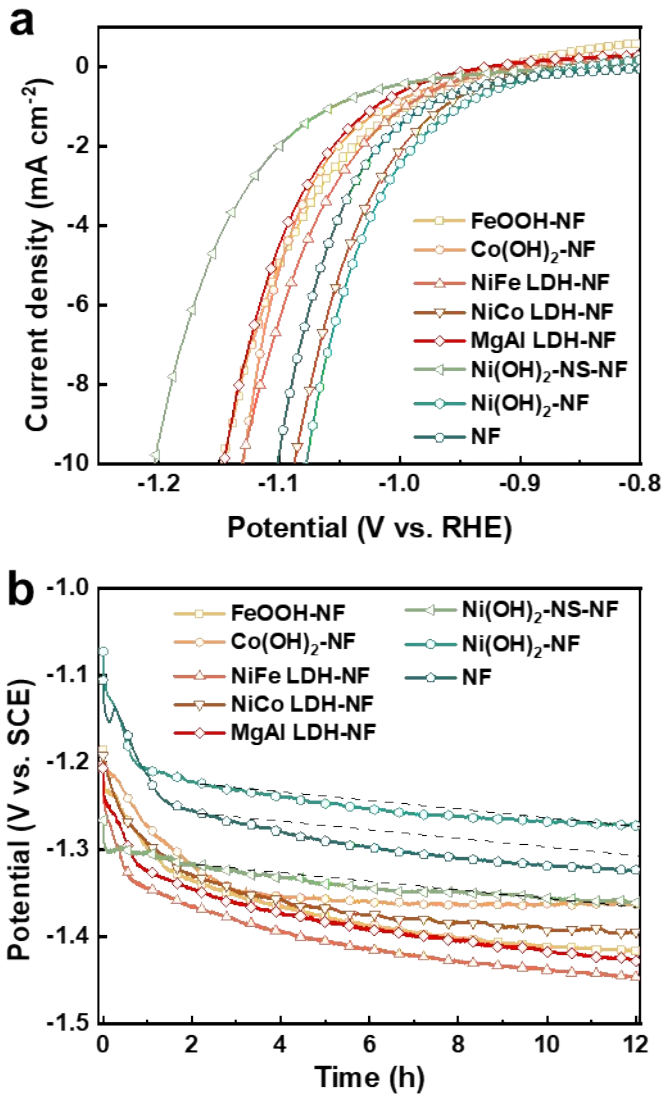

Fig. S19 (a) LSV and (b) chronopotentiometry curves of FeOOH-NF, $Co(OH)_2$-NF, Ni_2Fe_1 LDH-NF, Ni_2Co_1 LDH-NF, Mg_2Al_1 LDH-NF, $Ni(OH)_2$-NS-NF, $Ni(OH)_2$-NF and NF electrode in SW+$Mg(OH)_2$+AEM.

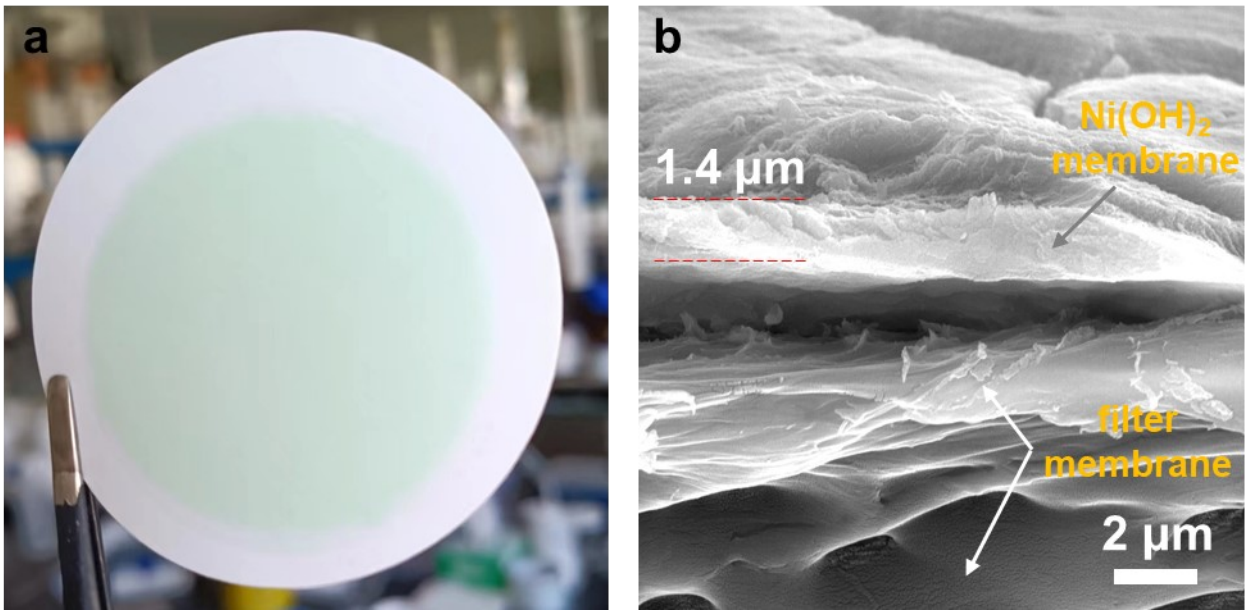

Fig. S20 (a) Photograph and (b) SEM image of $Ni(OH)_2$ membrane coated on nylon filter membrane.

The $Ni(OH)_2$ membrane was peeled off from abundant $Ni(OH)_2$-NF electrodes via ultrasound over 24 h, then centrifuged and washed with water for several times. The obtained $Ni(OH)_2$ was dispersed in water to store.

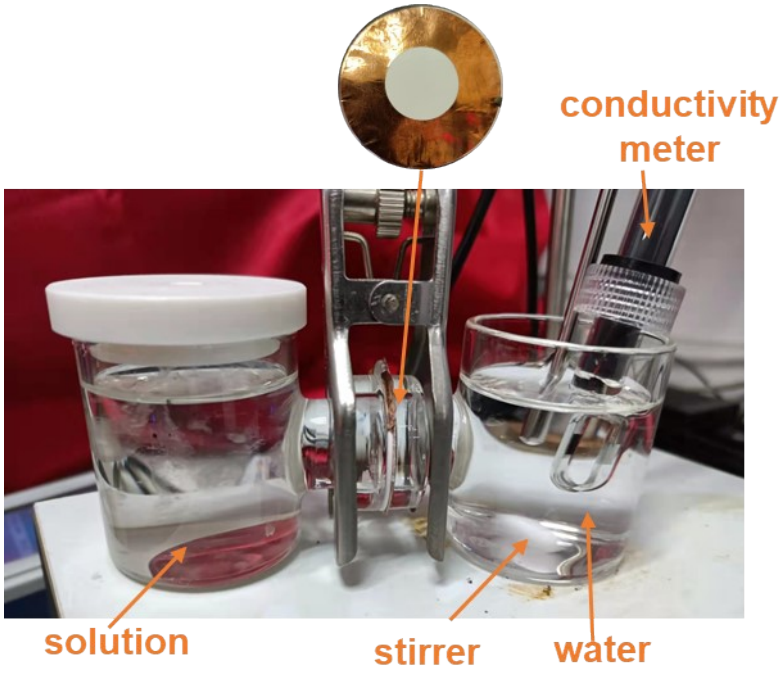

Fig. S21 Photograph of $Ni(OH)_2$ membrane test setup. The $Ni(OH)_2$ membrane was filtered on the nylon filter membrane, and sealed with a 2 cm^2 opening in copper (Cu) tape.

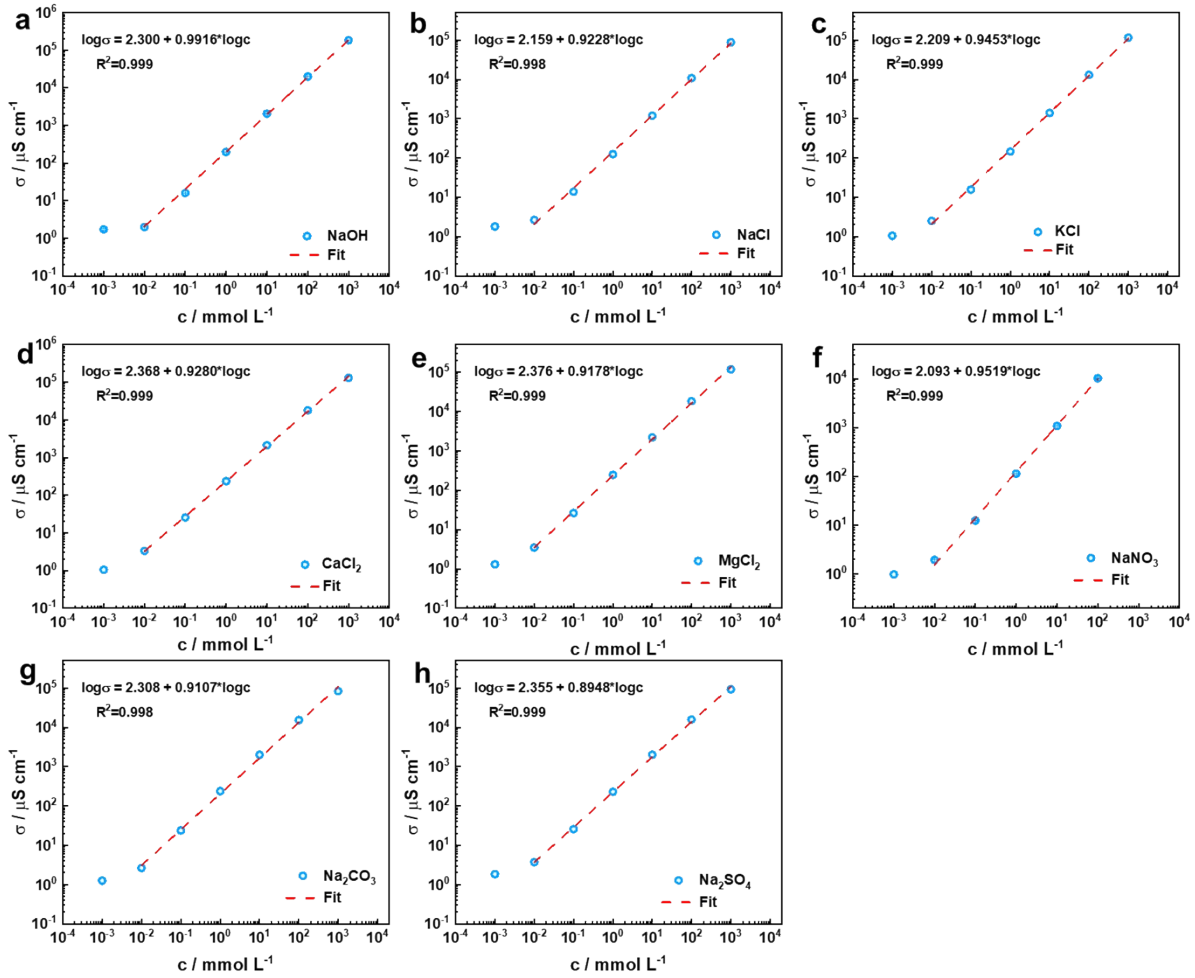

Fig. S22 The relationship between conductivity (σ) and concentration (c), lg(σ) = a + lg(c). (a) NaOH, (b) NaCl, (c) KCl, (d) $CaCl_2$, (e) $MgCl_2$, (f) $NaNO_3$, (g) Na_2CO_3, and (h) Na_2SO_4 solution.

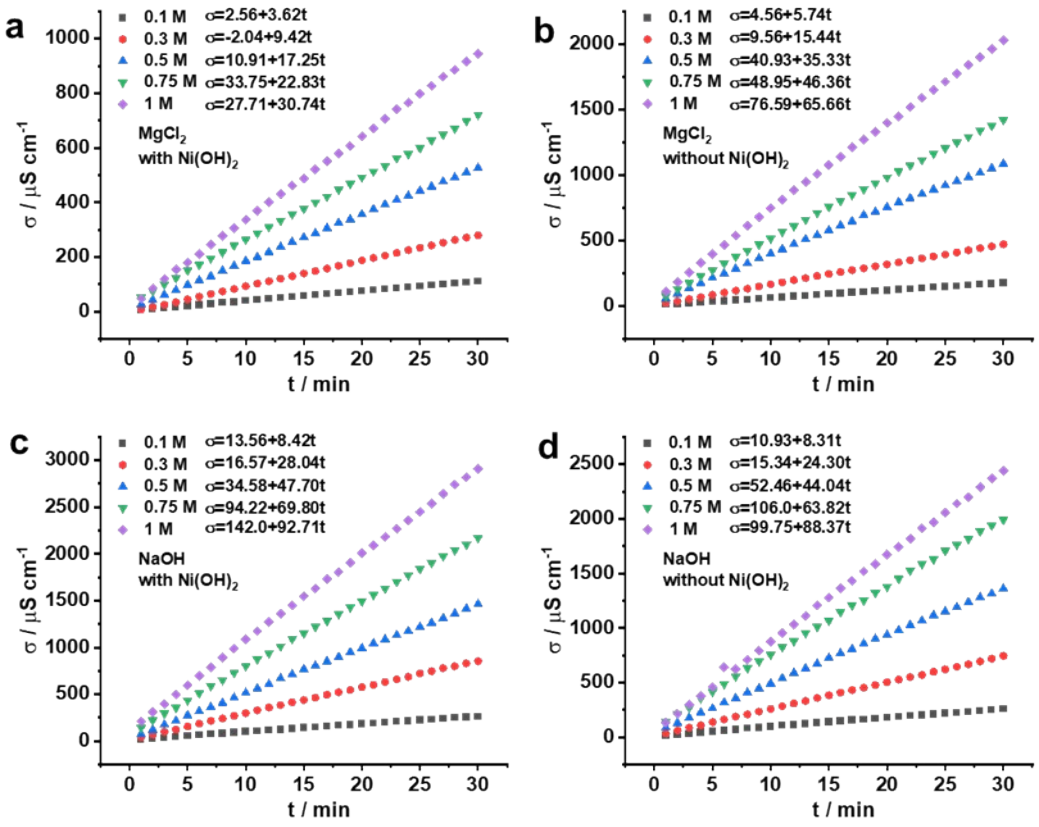

Fig. S23 The conductivity (σ) of $MgCl_2$ and NaOH solution with the measure time increase. The $MgCl_2$ solution through (a) the $Ni(OH)_2$ membrane coated substrate, and (b) nylon membrane substrate, NaOH solution through (c) the $Ni(OH)_2$ membrane coated substrate, and (d) substrate with concentration from 0.1 to 1 M.

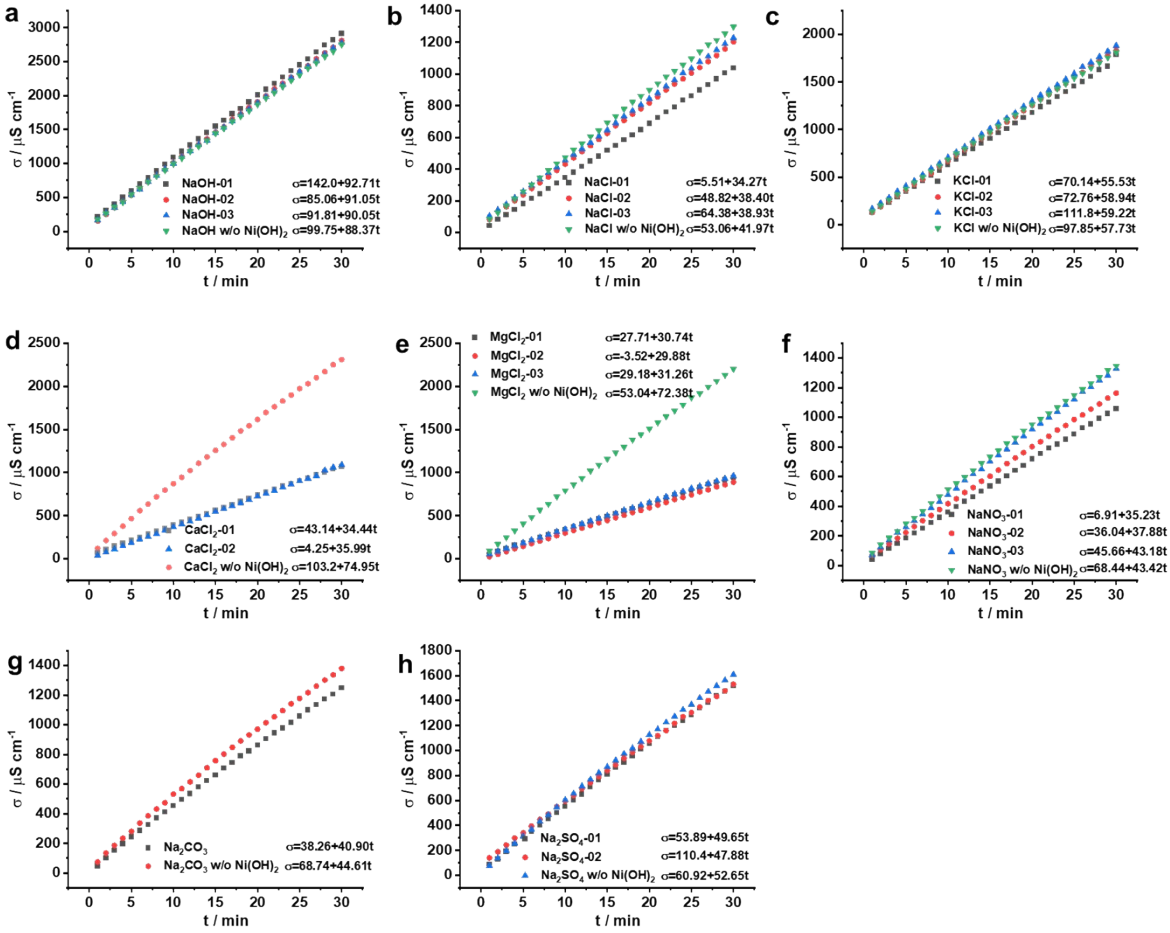

Fig. S24 The conductivity (σ) of the 1 M solutions with the measure time increase. (a) NaOH, (b) NaCl, (c) KCl, (d) $CaCl_2$, (e) $MgCl_2$. (f) $NaNO_3$, (g) Na_2CO_3, and (h) Na_2SO_4 solution through the $Ni(OH)_2$ membrane coated substrate, and nylon membrane substrate.

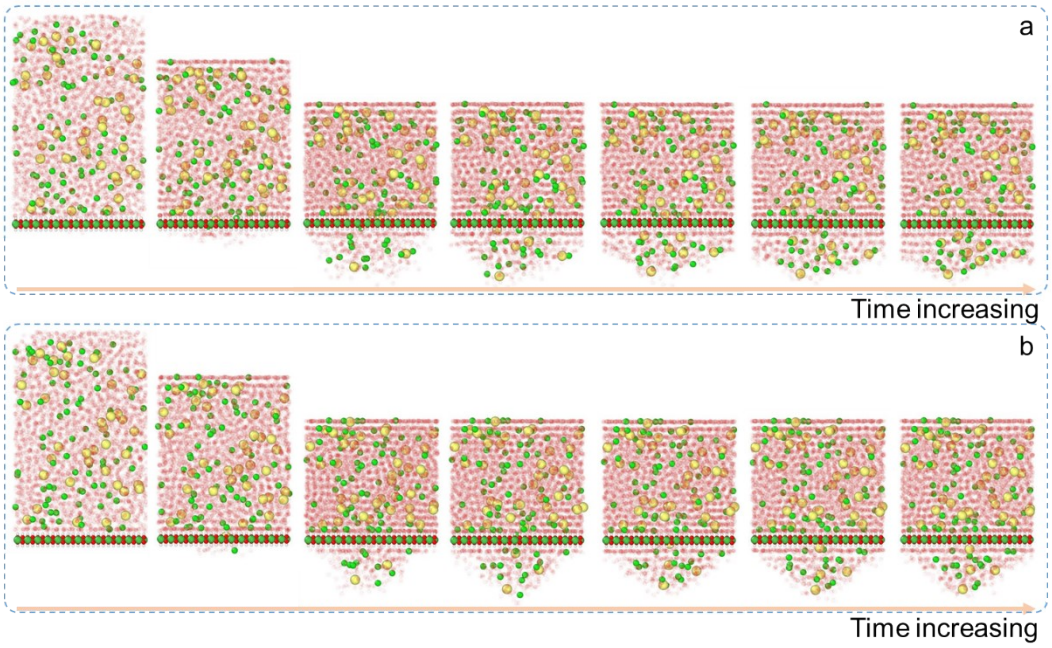

Fig. S25 Simulation snapshots of $MgCl_2$ solution through the opening monolayer $Ni(OH)_2$ nanosheet (a)without and (b) with positive charge.

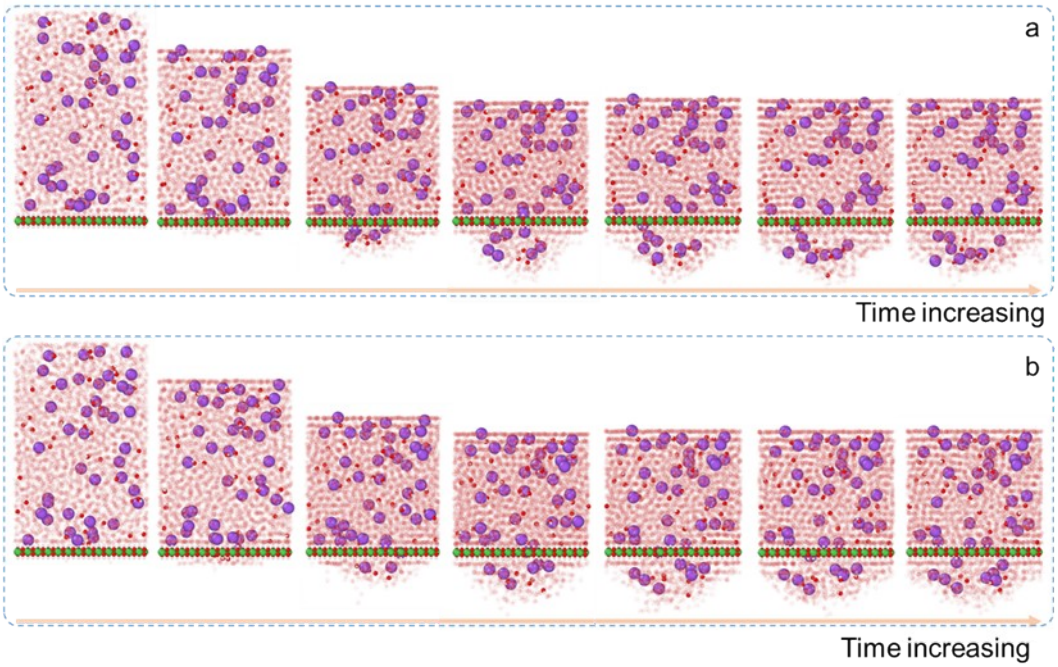

Fig. S26 Simulation snapshots of NaOH solution through the opening monolayer $Ni(OH)_2$ nanosheet (a)without and (b) with positive charge.

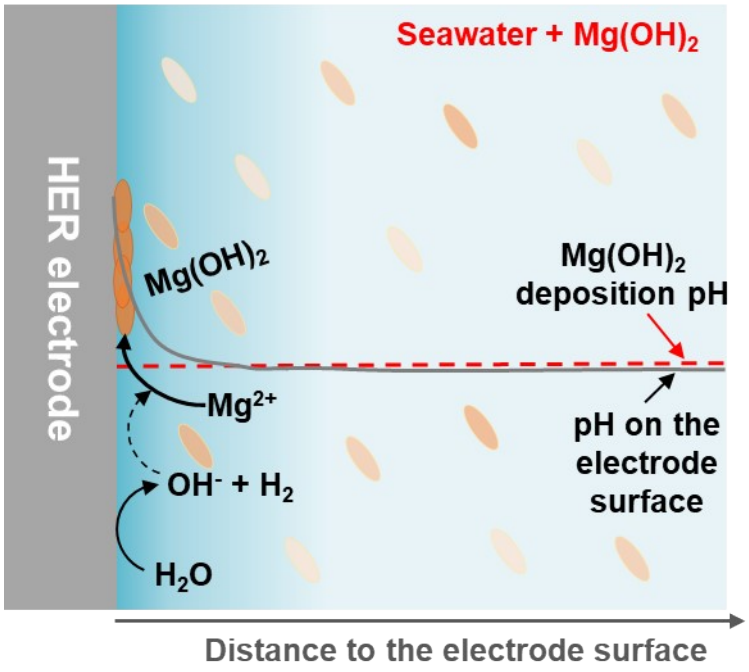

Fig. S27 The schematic illustration of precipitation mechanism on HER electrode without $Ni(OH)_2$ membrane in seawater with saturated $Mg(OH)_2$.

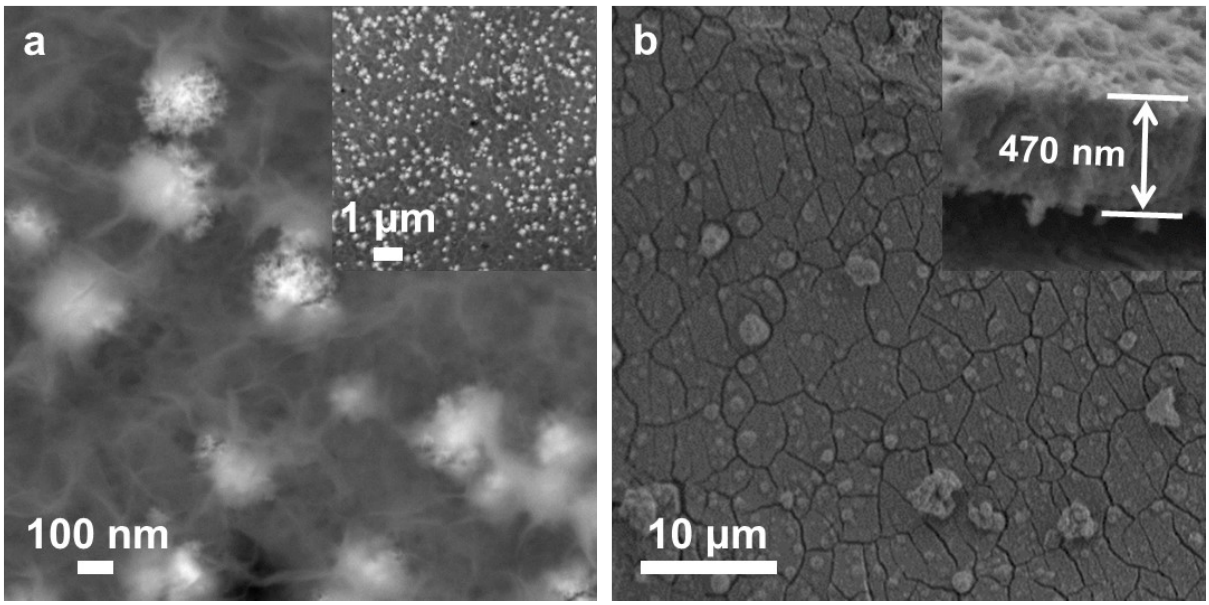

Fig. S28 SEM images of (a) Pt-NF electrode under backscattered electron image model, and (b) $Ni(OH)_2$-Pt-NF-3d electrode under secondary electron image model.

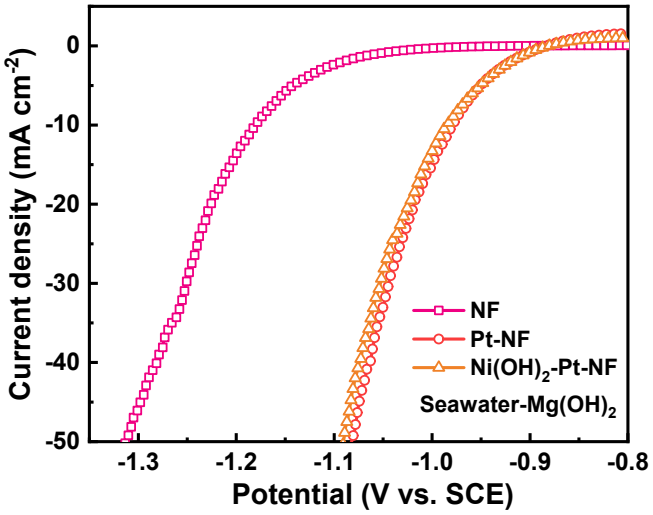

Fig. S29 LSV curves of NF, Pt-NF and $Ni(OH)_2$-Pt-NF electrode in seawater with saturated $Mg(OH)_2$.

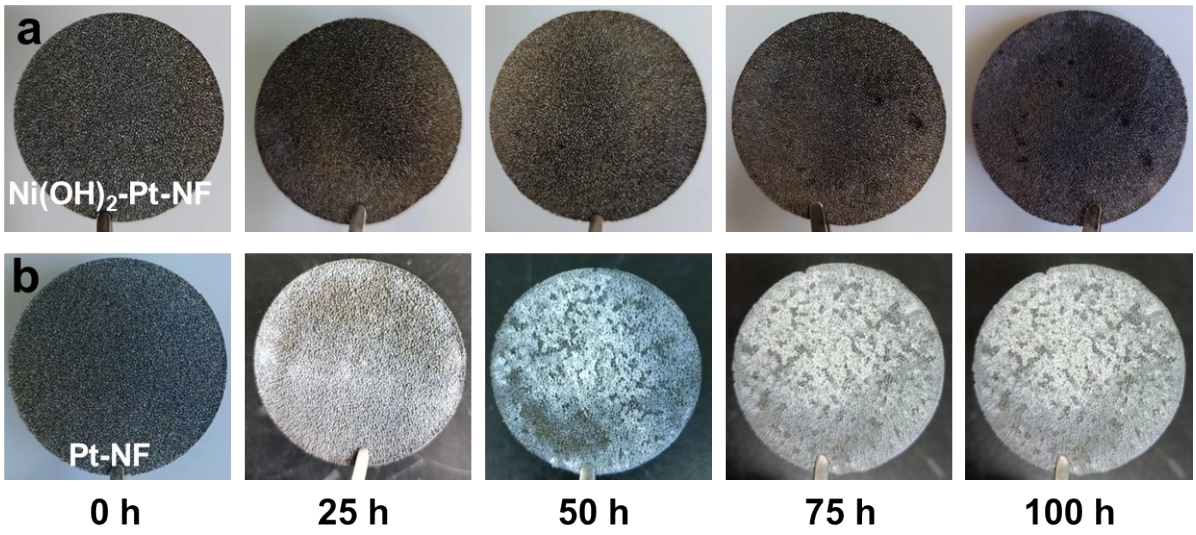

Fig. S30 Photographs of (a) $Ni(OH)_2$-Pt-NF and (b) Pt-NF electrodes before and after test in seawater electrolyser.

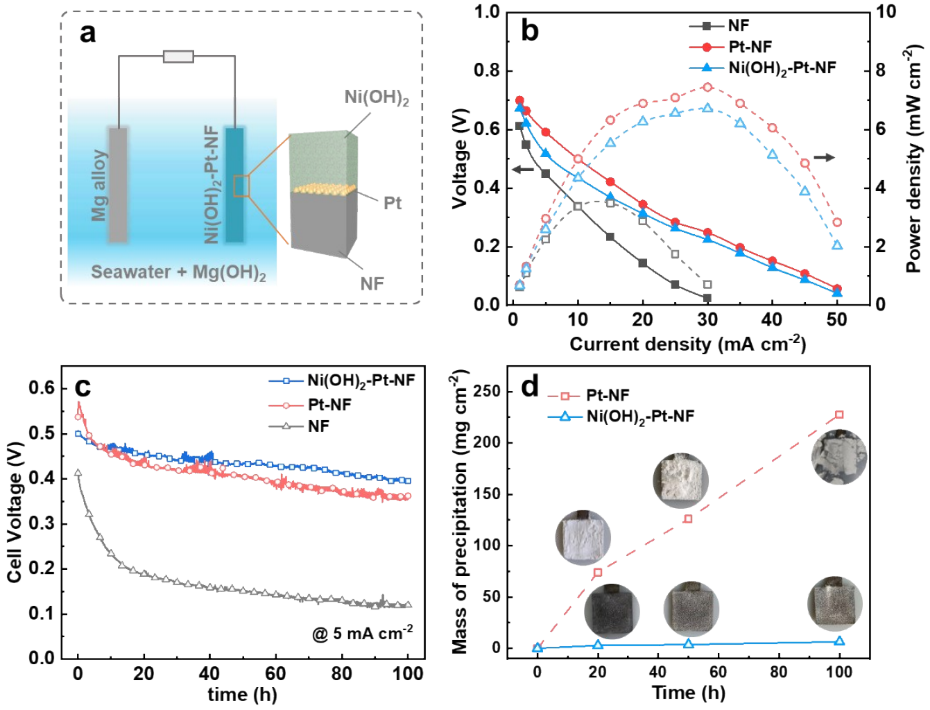

Fig. S31 (a) The schematic illustration of MSWB equipped with $Ni(OH)_2$-Pt-NF electrode. (b) The polarization and power density curves, (c) galvanostatic discharge of the MSWBs at current density of 5 mA cm^{-2} equipped with $Ni(OH)_2$-Pt-NF, Pt-NF, and NF electrodes. (d) Mass of precipitation on the $Ni(OH)_2$-Pt-NF, and Pt-NF electrode at different discharge time with the corresponding photographs.

To verified the anti-precipitation performance of the membrane decorated electrode in application, we also assembled the magnesium seawater battery (MSWB) equipped with $Ni(OH)_2$-Pt-NF cathode (HER electrode) and Mg alloy anode (Fig. S29a), which was tested in seawater with saturated $Mg(OH)_2$. Due to the high activity of Pt, the Pt-NF and $Ni(OH)_2$-Pt-NF electrode equipped MSWB exhibited higher performance than that of NF electrode (Fig. S29b). The highest output power density of MSWB equipped with $Ni(OH)_2$-Pt-NF and Pt-NF electrode was 6.71 and 7.45 mW cm^{-2} at 30 mA cm^{-2}, which was much higher than that of NF electrode (3.49 mW cm^{-2} at 15 mA cm^{-2}). For 100 h discharge at current density of 5 mA cm^{-2}, the Pt-NF electrode equipped MSWB exhibited higher discharge voltage than that of $Ni(OH)_2$-Pt-NF electrode during the initial operation (Fig. S29c). With the time increasing, the MSWB voltage of Pt-NF electrode decreased faster than that of $Ni(OH)_2$-Pt-NF electrode. At time of 6.5 h, they reached the same voltage, while at time of 100 h, the voltage of $Ni(OH)_2$-Pt-NF electrode equipped MSWB was 40 mV higher than that of Pt-NF electrode, and about 275 mV higher than that of NF electrode. As a comparation, the different operation time MSWBs were carried out. As shown in Fig. S29d, the precipitation mass on the electrode was increased with time both for $Ni(OH)_2$-Pt-NF and Pt-NF electrode equipped MSWBs. However, the precipitation mass on $Ni(OH)_2$-Pt-NF electrode was much lower than that of Pt-NF electrode. Such as at time of 100 h, the precipitation mass on $Ni(OH)_2$-Pt-NF electrode (6.43 mg cm^{-2}) was only 2.23% to Pt-NF electrode (288 mg cm^{-2}). It should be clarified that in the MSWB, the Mg alloy anode continuously supplied Mg^{2+} into the seawater during operation to increase the precipitation mass on the cathode as compared to three-electrode test with AEM. The results verified that the $Ni(OH)_2$ membrane on electrode can obviously decrease the electrode surface precipitation.

Table S1 Data analysis of the simulations.

		$MgCl_2$ solution			NaOH solution		
		Mg^{2+}	Cl^-	H_2O	Na^+	OH^-	H_2O
Number of particles through $Ni(OH)_2$ at 7 ns	0 charge	8	19	556	8	6	555
	+10 charge	4	16	435	8	6	531
Mass transfer rate* (No. ns^{-1})	0 charge	2.75	17.0	414	8.15	14.3	433
	+10 charge	1.16	15.7	383	5.90	13.7	378
Percentage transfer rate (% ns^{-1})**	0 charge	0.0687	0.212	0.138	0.204	0.357	0.144
	+10 charge	0.0291	0.196	0.128	0.147	0.342	0.126
Ionic diffusion coefficient* (cm^2 s^{-1})**		0.706	2.032	-	1.334	5.273	-

* Mass transfer rate was calculated from the slopes of passing number of the ions or water molecules with the time, when the ions or molecules passed through the $Ni(OH)_2$ sheet with relatively constant speed.

** Percentage transfer rate = Mass transfer rate / total number of the ion or molecular.

*** Data from handbook, W. M. Haynes, D. R. Lide, T. J. Bruno, CRC Handbook of Chemistry and Physics, 95th, CRC Press, Boca Raton 2014, p5-57.

References

1 Q. Liu, Z. Yan, J. Gao, E. Wang, G. Sun, *ACS Appl. Mater. Interfaces*, 2020, **12**, 24683-24692.
2 W.G. Hoover, *Phys. Rev. A*,1985, **31**, 1695-1697.
3 Q. Liu, X. Zhang, B.B. Jiang, J.F. Li, T. Li, X.Z. Shao, W.B. Cai, H.Y. Wang, Y.K. Zhang, *ACS Omega*, 2021, **6**, 14952-14962.
4 H. Li, J. Ma, D.G. Evans, T. Zhou, F. Li, X. Duan, *Chem. Mater.*, 2006, **18**, 4405-4414.
5 S. Plimpton, *J. Comput. Phys.*, 1995, **117**, 1-19.